Comparative Performance and Model Agreement of Three Common Photovoltaic Array Configurations

Matthew T. Boyd
National Institute of Standards and Technology (NIST),
100 Bureau Drive,
Gaithersburg, MD 20899
e-mail: matthew.boyd@nist.gov

Three grid-connected monocrystalline silicon arrays on the National Institute of Standards and Technology (NIST) campus in Gaithersburg, MD have been instrumented and monitored for 1 yr, with only minimal gaps in the data sets. These arrays range from 73 kW to 271 kW, and all use the same module, but have different tilts, orientations, and configurations. One array is installed facing east and west over a parking lot, one in an open field, and one on a flat roof. Various measured relationships and calculated standard metrics have been used to compare the relative performance of these arrays in their different configurations. Comprehensive performance models have also been created in the modeling software PVSYST for each array, and its predictions using measured on-site weather data are compared to the arrays' measured outputs. The comparisons show that all three arrays typically have monthly performance ratios (PRs) above 0.75, but differ significantly in their relative output, strongly correlating to their operating temperature and to a lesser extent their orientation. The model predictions are within 5% of the monthly delivered energy values except during the winter months, when there was intermittent snow on the arrays, and during maintenance and other outages. [DOI: 10.1115/1.4038314]

Keywords: photovoltaic (PV) array, data acquisition, performance, PVSYST model, solar, temperature

1 Introduction

Three grid-connected solar photovoltaic (PV) arrays were constructed on the National Institute of Standards and Technology (NIST) campus in Gaithersburg, MD, with construction finishing around July 2012. This location is 32 km (20 mi) northwest of Washington, DC in a mixed-humid, subtropical climate zone [1] having four distinct seasons. Skies are variable, with only a couple days of cloudless skies per month, and the solar resource for PV is about (1600–1800) kWh/m^2/yr [2].

The three arrays on campus use the same monocrystalline silicon module, but all are mounted in different configurations: the canopy array (Fig. 1) is mounted on east and west facing canopies over a parking lot, the ground array (Fig. 2) is mounted on south-facing tilted ground supports in an open field, and the roof array (Fig. 3) is mounted on south-facing tilted, weighted racks on a flat building roof. There is a single inverter at each array, which is connected to the NIST campus grid, and subsequently the local grid. A summary of the arrays is given in Table 1, with descriptions of the array constructions and data acquisition systems given in Refs. [3] and [4], respectively.

Contributed by the Solar Energy Division of ASME for publication in the JOURNAL OF SOLAR ENERGY ENGINEERING: INCLUDING WIND ENERGY AND BUILDING ENERGY CONSERVATION. Manuscript received March 3, 2017; final manuscript received September 26, 2017; published online November 14, 2017. Assoc. Editor: Geoffrey T. Klise.

The arrays have been monitored since Aug. 1, 2014, with various irradiance, temperature, DC, and AC electrical measurements saved every 1-s, as described in Ref. [5]. An onsite weather station has provided supplementary beam, diffuse, total, and spectral irradiance measurements along with other more standard meteorological measurements, also saved every 1-s, as described in Ref. [6].

2 Data

The PV arrays continue to be monitored at the time of this writing, but the focus of the following analyses is from Oct. 1, 2014 to Sept. 30, 2015, chosen to be after some minor instrumentation

Fig. 1 Canopy array

Fig. 2 Ground array

Fig. 3 Roof array

Table 1 Summary of the campus PV arrays

	Canopy	Ground	Roof
Array-rated DC power (kW)	243	271	73
Latitude (°N)	39.1385	39.1319	39.1354
Longitude (°E)	−77.2155	−77.2141	−77.2156
Elevation[a] (m) (ft)	137 (450)	138 (453)	149 (489)
Height[b] (m) (ft)	5.11 (16.8)	0.67 (2.2)	0.08 (0.3)
Tilt (deg)	5	20	10
Azimuth (° CW from N.)	90,270	180	180
Number of modules	1032	1152	312
Module technology	Monocrystalline silicon—front contact		
Module-rated power (W)		235	
Modules per string		12	
Number of source circuits	86	96	26
Number of combiner boxes	7	7	4
Number of inverters	1	1	1
Inverter-rated power (kW)	260	260	75

[a]Elevation of the array support (e.g., ground, roof) above sea level.
[b]Height of bottom edge of the bottom module above the array support (e.g., ground, roof).

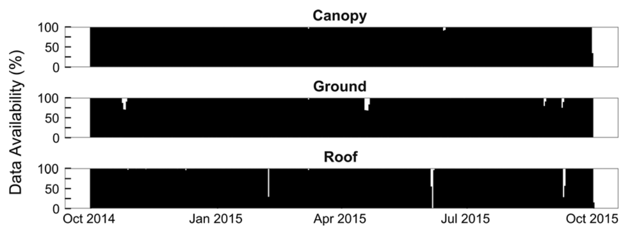

Fig. 4 The data availability for the three arrays. The black bars show the percent of the available data that is needed for a complete performance analysis. The data have been filtered to exclude invalid values.

bugs were resolved. Figure 4 illustrates gaps in the data sets during this time period, showing the daily percent of the available data needed for a complete performance analysis, which was chosen to include the following:

- Plane-of-array (POA) irradiance measured by a reference cell in all planes (canopy array has two)
- ambient temperature measured at the array
- module backside temperature, at least one in the center of a module
- wind speed and direction at the array
- DC voltage and current of the entire array
- AC voltage and current at the inverter or the local grid connection

The aggregate percent data availability for each array is greater than 99%, with the lost data usually due to an electrical maintenance outage or a failed inverter communication module. The instruments and sensors used to take the measurements in this analysis, and their corresponding uncertainties, are given in Table 2.

Summary plots of various measurements and metrics of the three arrays are shown in Fig. 5. These time series plots are for an arbitrarily selected week in the 1-yr period, starting on Apr. 26, 2015, when there were varying sky conditions, no array faults, and little to no precipitation. The data points are 1-min averages of the 1-s measurements.

The cell temperature was calculated by adding 0.9 °C to the measured backside temperature measurement, based on the mounting techniques and subsequent offsets measured by Smith et al. [7]. The normalized AC power is simply the AC power divided by the sum of the standard test condition (STC) rated DC power of the modules in the array. The performance ratio (PR) is a measure of how closely the array is operating relative to its aggregate module nameplate rating. It factors in all of the losses in the array, which include module shading, soiling, reflection, mismatch, wiring losses, inverter efficiency, failures and other system downtime, and the effects of the module cell temperature. PR is calculated using the following equation [8]:

$$\mathrm{PR} = \frac{\sum_i P_{\mathrm{AC},i}}{\sum_i \left[P_{\mathrm{STC}}\left(\frac{G_{\mathrm{POA},i}}{G_{\mathrm{STC}}}\right)\right]}$$

where P_{AC} is the generated AC power of the array in kW, i is the data index, P_{STC} is the combined rated DC power of the array modules at STC in kW, G_{POA} is the POA irradiance in W/m^2, and G_{STC} is the irradiance at STC, which is 1000 W/m^2.

The time series plots illustrate the higher irradiance on the ground array due to its more optimal orientation and tilt than the other two arrays, as it faces due south with its tilt closer to the site latitude. The temperature of the roof array is significantly higher than the other two even with lower irradiance, likely due to the installed wind deflectors insulating the backsides of the modules and the 14 story light colored and reflective building north of the array that augments the irradiance, mostly on its backside. The ground array shows more DC voltage spikes in the middle of the day and lower normalized power for three of those days. This occurs during times of higher irradiance and lower temperature, when the inverter reaches its power limit and has to adjust its maximum power point to reduce the input power. This adjustment occasionally results in a brief (≈15 s) no-power idle state. This power clipping does not occur for the other two arrays as the inverters are more oversized, and the arrays are not as optimally oriented. The PR plots show the characteristic dip in the middle of the day caused by the higher operating temperatures and corresponding lower efficiency.

Additional plots of selected correlations over the entire first year of monitoring are shown in Fig. 6. The data points are 1-min averages of the 1-s measurements and are binned in hexagonal areas to show the relative number of points. The number of data

Table 2 The instruments and sensors used in this analysis and the corresponding measurement uncertainties

	Instrument/sensor	Standard uncertainty
POA irradiance	Reference cell	5%
Module backside temperature	Resistance temperature detector	±0.5 °C
Ambient temperature	Resistance temperature detector in a passively ventilated radiation shield	±0.3 °C
DC voltage	Voltage divider	0.1%
DC power	Inverter	Unspecified
AC power (at inverter)	Inverter	Unspecified
AC power (at switchgear)	Power meter	5%

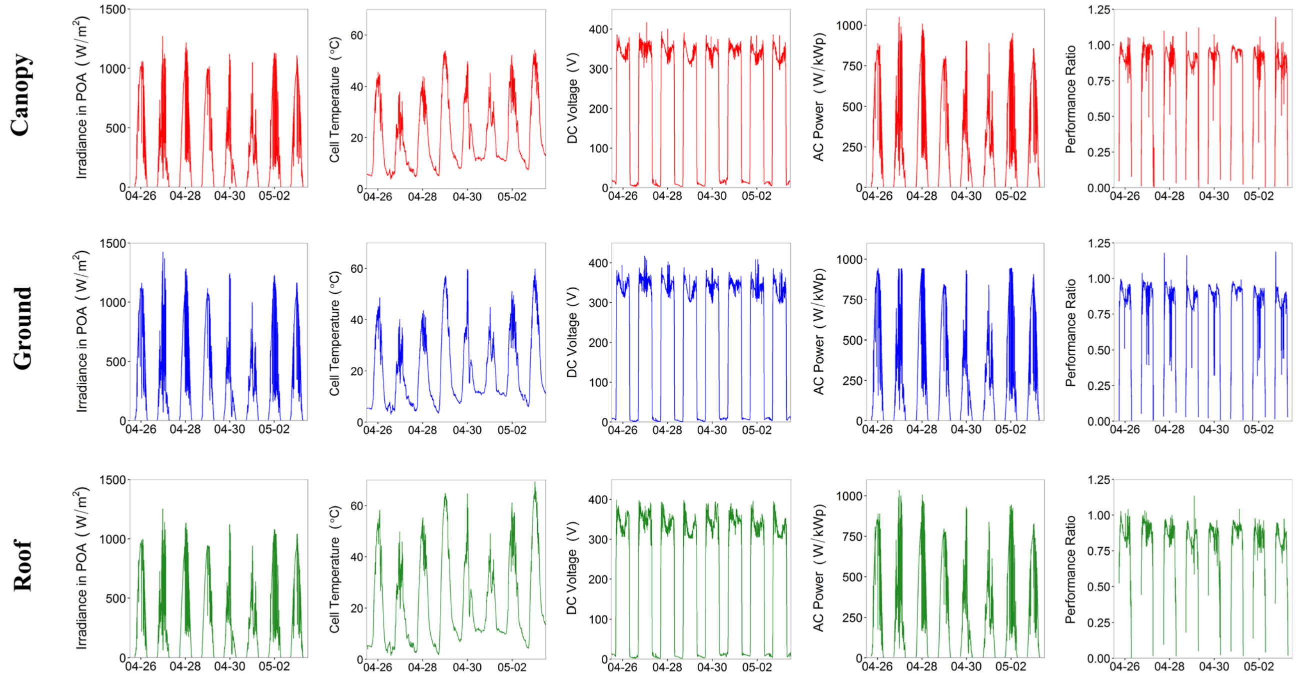

Fig. 5 Time series plots of selected measurements and metrics of the three arrays for the week starting on Apr. 26, 2015, when there were varying sky conditions, no array faults, and little to no precipitation. The AC power is normalized to the sum of the STC-rated DC power of the modules in the array.

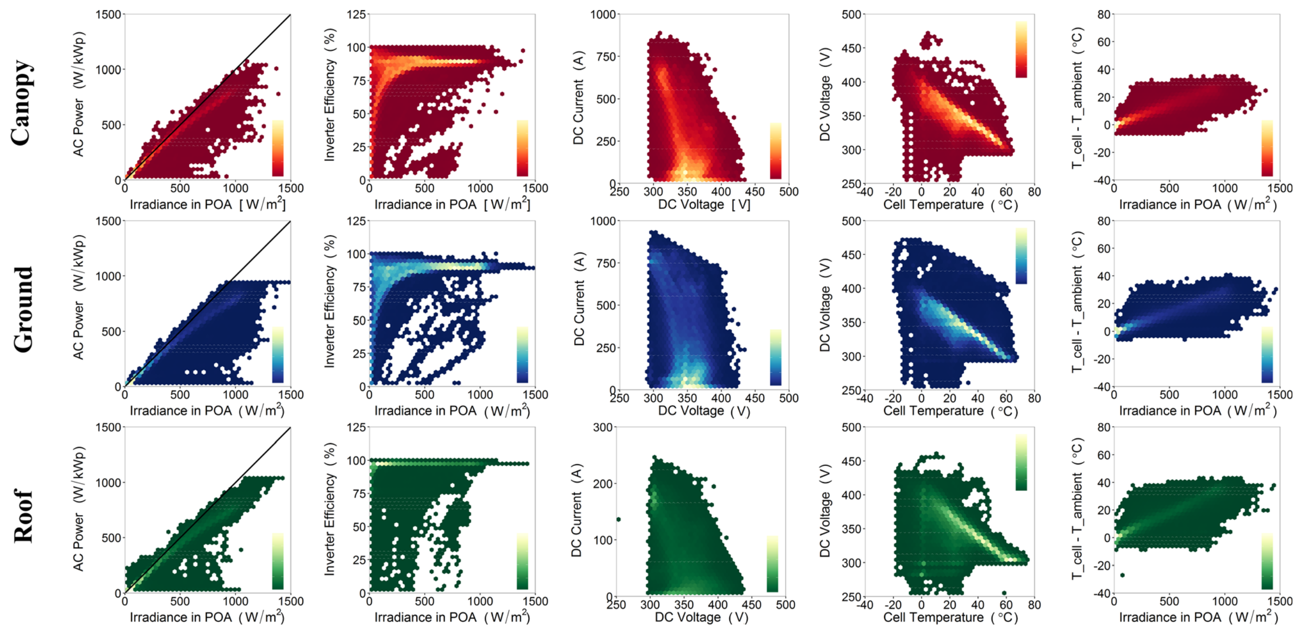

Fig. 6 Hexagonally binned scatter plots of the same measurements and metrics shown in Fig. 5, but for the entire first year of monitoring, from Oct. 1, 2014 to Sept. 30, 2015. The AC power is normalized to the sum of the STC-rated DC power of the modules in the array, and the inverter efficiency is simply the AC power divided by the DC power. Note that the *y*-axis in the DC current versus DC power plot is scaled-up for the roof array.

points in each hexagonal grid space is indicated by the intensity of the grid space color, with lighter colors indicating more points.

In the far left plots, the ground array shows a larger spread in AC power toward lower values due to the more time it was operating with a portion of the array off. The lower slope in the plot for the roof array also shows the lower efficiency from the higher operating temperatures. This lower efficiency is not due to the inverter, which actually shows a higher efficiency at these irradiances than the other two inverters due to its better sizing, as shown in Table 1. The wider spread in DC voltage in the third roof array plot could be due to the array's more variable temperature from the added irradiance heating. The notable absence of observations less than $\approx$300 V and greater than $\approx$30 °C in the fourth column of DC voltage versus cell temperature plots is simply due to it being a time of low-irradiance, where the inverters' power tracking lower cutoffs are $\approx$300 V and the cell

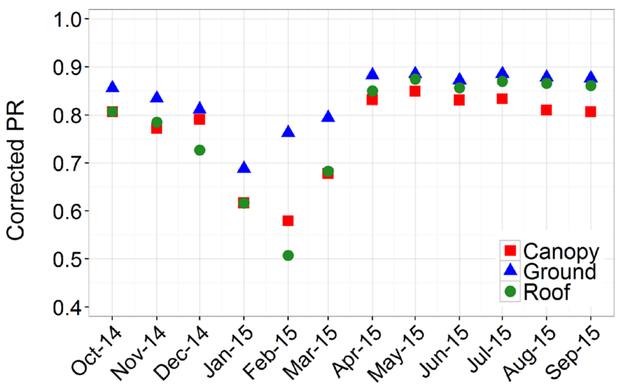

Fig. 7 The temperature corrected PRs of the arrays during the first year of monitoring

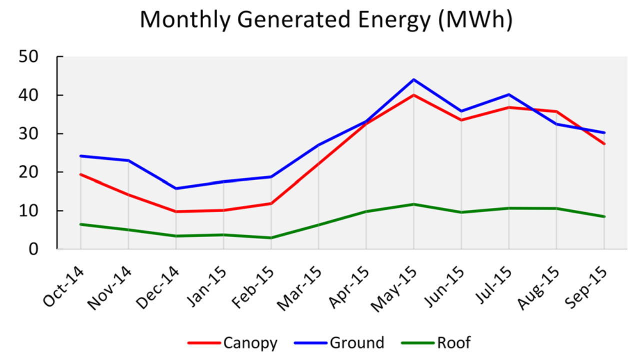

Fig. 8 The monthly energies delivered to the local grid by the arrays for the first year of monitoring

temperatures not rising much above the ambient temperatures. Finally, in the far right column of plots, the roof array shows a much higher correlation between the temperature rise of the modules and the POA irradiance, as previously discussed and illustrated in the time series plots.

3 Summary Statistics

The temperature-corrected performance ratio was calculated to reduce the seasonal biases in the traditional performance ratio metric in order to get more consistent comparisons throughout the year. The bias is caused by the inverse relationship between module cell temperature and efficiency and is lowest in the summer when the combined ambient temperature and amount of light being absorbed by and heating the modules is highest. The bias is the highest in the winter when the opposite is occurring. This metric aims to reduce these variations by normalizing the temperature effect to that at the yearly average module cell temperature. The corrected performance ratio is calculated using the following equation [8]:

$$\mathrm{PR}_{\mathrm{corr}} = \frac{\sum_i P_{\mathrm{AC},i}}{\sum_i \left[P_{\mathrm{STC}} \left(\frac{G_{\mathrm{POA},i}}{G_{\mathrm{STC}}} \right) \left(1 - \frac{\delta}{100} \left(T_{\mathrm{cell,avg}} - T_{\mathrm{cell},i} \right) \right) \right]}$$

where P_{AC} is the AC power generated by the array in kW, i is the data index, P_{STC} is the combined rated DC power of the array modules at STC in kW, G_{POA} is the POA irradiance in W/m^2, G_{STC} is the irradiance at STC (1000 W/m^2), δ is the module cell temperature coefficient in %/°C, $T_{\mathrm{cell,avg}}$ is the average yearly module operating cell temperature in °C, and T_{cell} is the module cell temperature in °C. Times during the night and when the array is nonoperational are excluded. A plot of the monthly corrected PR is shown in Fig. 7, and a plot of the monthly generated energies is shown in Fig. 8. Due to the two module orientations in the canopy array, the average of the two POA irradiances was used in the calculations.

The monthly performance ratio plot shows that the arrays perform reasonably well except during the winter months when snow was often present on the arrays. PR values for new systems typically are in the range of 0.6–0.9 [9], so it appears from this plot that there were not any significant problems with the arrays. The ground array consistently generated the most energy, except in August of 2015 when there was an arcing event in the inverter's DC combiner compartment that brought down the array for the last week of the month. This event is not apparent in the plot of the performance ratios, because times when the arrays are off are excluded.

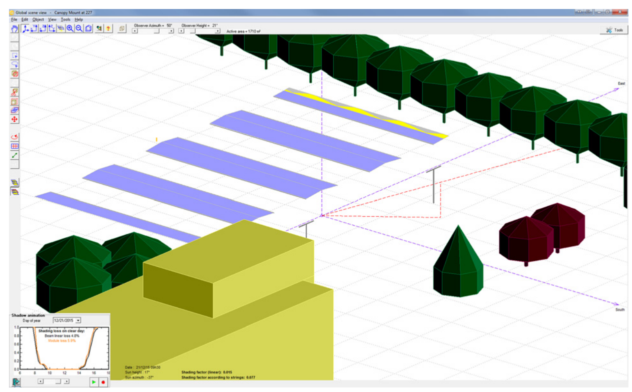

Fig. 9 The CAD model for the canopy array used for modeling the effect of near shading on the array performance, showing shading on the east canopy at 09:30 am on the winter solstice. The gray triangular areas on the right of the far right canopy indicate shading, and along with the adjacent triangles indicate nonoperating modules.

4 Modeling

The three PV arrays were modeled in PVSYST [10],[1] a software package that uses a semi-empirical equivalent circuit model. Weather data for the model simulations were measured onsite. The horizon shading was modeled using hemispherical image projections of the site, and the near shading was modeled using full computer-aided design (CAD) layouts of the arrays and immediate surroundings. The CAD model of the canopy array is shown in Fig. 9. The individual module electrical connections were specified, and the wiring losses were calculated from construction drawing values. The PV module and inverter specification files were obtained from the built-in database and directly from the manufacturer, respectively. Other, lower-level, model inputs were left at their default values. The snow on the arrays and its effect on the local albedo were not accounted for due to its partial and intermittent coverage.

The predicted hourly average powers delivered to the grid are compared to the measured powers, as shown in Fig. 10. The values shown are power, in kW, but they are also equal to the integrated hourly energy, in kWh. The residuals (modeled minus measured) are scaled by the rated DC powers of the arrays at STC. Values during nighttime are removed, and the residual plots are cropped to the same values for each array to exclude when they were either fully or partially offline.

[1] Certain commercial equipment, instruments, or materials are identified in this paper to foster understanding. Such identification does not imply recommendation or endorsement by the National Institute of Standards and Technology, nor does it imply that the materials or equipment identified are necessarily the best available for the purpose.

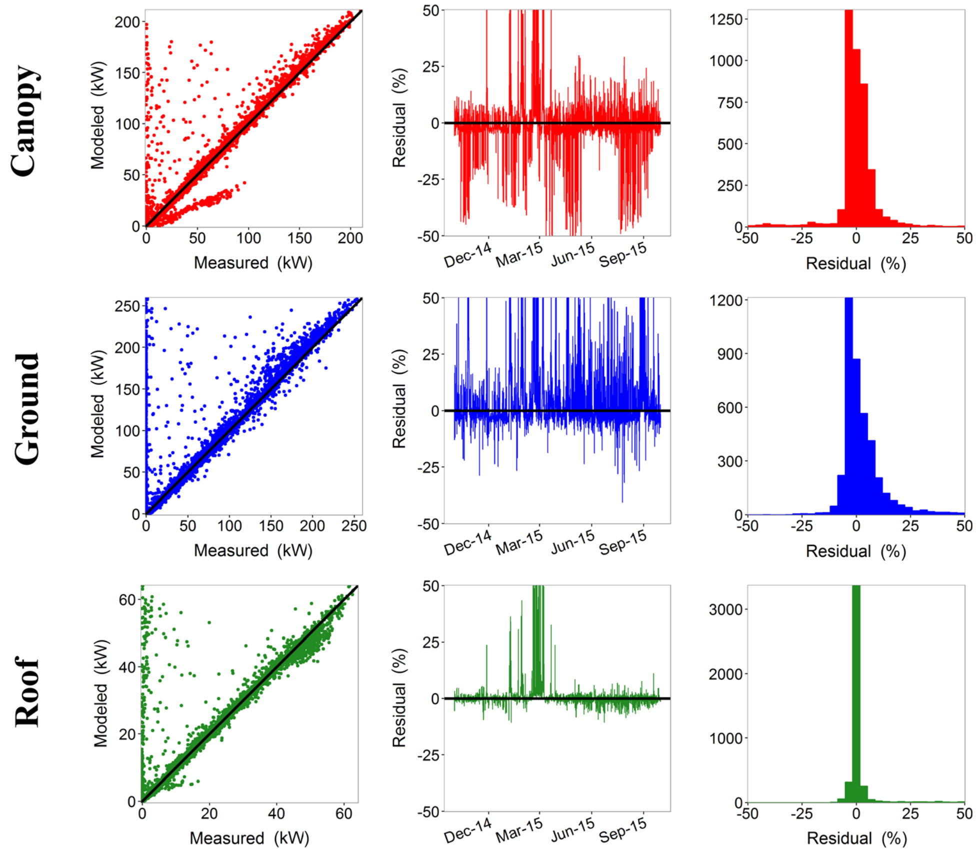

Fig. 10 Modeled versus measured power delivered to the grid and their residuals (modeled minus measured) at an hourly time-step for the three arrays for the entire first year of monitoring, from Oct. 1, 2014 to Sept. 30, 2015. The residuals are normalized to the DC power of the arrays at STC, and these values are cropped to exclude when the arrays were either fully or partially offline.

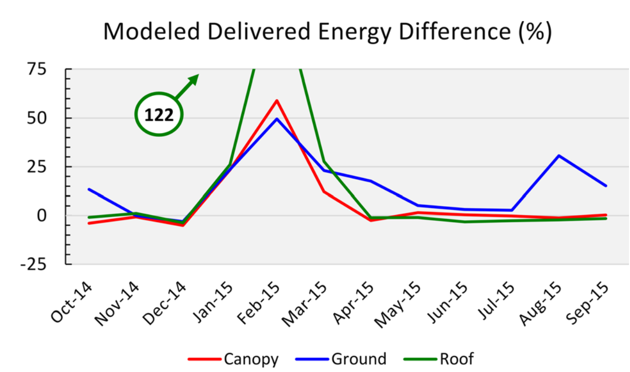

Fig. 11 Model deviations for the monthly delivered energy predicted by PVSYST for the three arrays. Positive values indicate model over-prediction.

The powers predicted by the model show generally good agreement to the measurements, with the best fit for the roof array. Values when the arrays were offline are apparent and indicated by the values along the *y*-axis in the left column of plots and by the large positive spikes in the middle column of plots. The data along the lower sloped line in the first plot for the canopy array occur almost entirely before 8:00 EST and after 15:00 EST and are due to the model predicting shading on the east and west-most canopies when there is none. The residuals for the canopy and ground arrays have some positive skew, as shown in the right column of histograms, indicating more model over-prediction than under-prediction. These over-predictions could be from the arrays under-performing due to maintenance outages, degradation, or component failures.

Differences between the modeled and measured delivered energies for the three arrays, plotted in Fig. 11, show large deviations for the winter months when the arrays had intermittent snow

Table 3 Measured yearly delivered energy and the deviations from the PVSYST model for the three arrays. Positive values indicate model over-prediction.

Array	Measured energy (MWh)	Model residual (MWh)	Modeled percent difference (%)
Canopy	293.4	10.2	3.5
Ground	342.1	47.3	13.8
Roof	88.6	5.0	5.6

cover. There are also substantial model over-predictions for October 2014 and April 2015 for the ground array, which are times when the array was off for two to three days for building switchgear maintenance. The over-prediction for August 2015 is due to the arcing event described early in Sec. 3. Otherwise, the percent differences are less than approximately 5%. The total annual model deviations are given in Table 3.

5 Conclusion

The three largest PV arrays on the NIST campus in Gaithersburg, MD have demonstrated good performance for 1 yr of operation. There are no indications of any systemic problems, with the data acquisitions systems capturing over 99% of this operation period at a 1-s resolution. The largest array, installed in an open field, exhibits some power clipping by the inverter due to it being slightly undersized relative to its DC-rated power. This array, however, still consistently has the highest performance ratio due to its more optimal orientation than the east/west oriented array over the parking lot and its lower operating temperature than the backside-covered array located on the roof. The rooftop array, the smallest of the three arrays, has the highest operating temperatures likely because of less airflow behind the modules and higher backside radiation from reflections off a building to its north. This negative effect is somewhat offset by having the highest inverter efficiency out of the three arrays, due partly to its sizing. Excluding times of snow coverage and partial and full outages, all arrays exhibit high monthly performance ratios between 0.75 and 0.9. Monthly generated energies are consistently proportionate between the arrays except during months when there are array outages. During normal operating periods, the PVSYST model predictions are all within 5% of the measured powers, but the differences increase drastically during outages and periods of snow coverage.

References

[1] Peel, M. C., Finlayson, B. L., and McMahon, T. A., 2007, "Updated World Map of the Köppen-Geiger Climate Classification," Hydrol. Earth Syst. Sci., **11**(5), pp. 1633–1644.

[2] NREL, 2016, "NREL: Dynamic Maps, GIS Data, and Analysis Tools," National Renewable Energy Laboratory, Golden, CO, accessed Sept. 19, 2016, https://www.nrc.gov/docs/ML1409/ML14093A281.pdf

[3] Dougherty, B., and Boyd, M., 2016, "Model (at Least) Twice, Build Once: Experiences With the Design-Bid-Build Process for Solar Photovoltaic Arrays," ASME J. Sol. Energy Eng., **139**(3), p. 035001.

[4] Boyd, M., 2016, "High-Speed Monitoring of Multiple Grid-Connected Photovoltaic Array Configurations and Supplementary Weather Station," ASME J. Sol. Energy Eng., **139**(3), p. 034502.

[5] Boyd, M., 2015, "High-Speed Monitoring of Multiple Grid-Connected Photovoltaic Array Configurations," National Institute of Standards and Technology, Gaithersburg, MD, Technical Note No. 1896.

[6] Boyd, M., 2016, "NIST Weather Station for Photovoltaic and Building System Research," National Institute of Standards and Technology, Gaithersburg, MD, Technical Note No. 1913.

[7] Smith, R. M., Kurtz, S., and Sekulic, B., 2011, "Back-of-Module Temperature Measurement Methods," SolarPro, **4**(6), pp. 90–104.

[8] Dierauf, T., Growitz, A., Kurtz, S., Cruz, J. L. B., Riley, E., and Hansen, C., 2013, "Weather-Corrected Performance Ratio," National Renewable Energy Laboratory, Golden, CO, Technical Report No. NREL/TP-5200-57991.

[9] Marion, B., Adelstein, J., Boyle, K., Hayden, H., Hammond, B., Fletcher, T., Canada, B., Narang, D., Shugar, D., Wenger, H., Kimber, A., Mitchell, L., Rich, G., and Townsend, T., 2005, "Performance Parameters for Grid-Connected PV Systems," IEEE Conference Record of the Thirty-First Photovoltaic Specialists Conference (PVSC), Lake Buena Vista, FL, Jan. 3–7, pp. 1601–1606.

[10] Mermoud, A., 2016, "PVsyst v6.4.1," PVsyst SA, Satigny, Switzerland.